

# OPTICAL SPECTRUM OF MAIN-, INTER- AND OFF-PULSE EMISSION FROM CRAB PULSAR

Alberto Carramiñana<sup>1</sup>, Andrej Čadež<sup>2</sup>, Tomaž Zwitter<sup>2</sup>

## ABSTRACT

A dedicated stroboscopic device was used to obtain optical spectra of the Crab main-pulse and inter-pulse as well as the spectrum of the underlying nebula when the pulsar is turned off. As the nebular emission is very inhomogeneous, our ability to effectively subtract the nebular background signal is crucial.

No spectral lines intrinsic to the pulsar are detected. The main-pulse and the inter-pulse behave as power laws, both with the same de-reddened index  $\alpha = +0.2 \pm 0.1$ . This value was obtained by subtracting the nebular spectrum at the exact position of the pulsar. The underlying nebula is redder,  $\alpha = -0.4 \pm 0.1$ . Its emission lines are split into approaching ( $\sim -1200$  km/s) and receding ( $\sim +600$  km/s) components. The strength of emission line components and the flux in nebular continuum vary on arcsec scale. The nebular line and continuum intensities along the N-S slit are given.

*Subject headings:* Pulsars: individual (PSR B0531+21) — stars: neutron — techniques: spectroscopic — supernova remnants

## 1. Introduction

The Crab pulsar (PSR J0534+2200 = PSR B0531+21) was the first pulsating radio source identified at optical wavelengths (Cocke, Disney, & Taylor 1969; Lynds, Maran, & Trumbo 1969). Most subsequent studies concentrated on the pulse shape in various photometric bands (Percival et al. 1993; Eikenberry et al. 1996; Perryman et al. 1999; Lundqvist et al. 1999). They generally suggested small color variations in the light curve. No spectroscopic data existed until Nasuti et al. (1996) obtained the first optical spectrum. They were able to measure the general flux distribution as well as hint to an unidentified intrinsic absorption feature at 5920 Å. Their spectrum is phase averaged, so no information on spectral variation with pulse phase can be extracted.

Here we present the first flux-calibrated optical spectrum, separately for the main-pulse, the inter-pulse and the off-pulse components. The spectra of both pulses are compared with phase-resolved photometric studies. Except for a very small ( $\sim 1\%$ ) contribution from the pulsar (Golden et al. 2000), the off-pulse spectrum, also presented here, corresponds to the nebular emission along the line of sight of the pulsar.

---

<sup>1</sup>I.N.A.O.E., Luis Enrique Erro 1, Tonantzintla, Puebla 72840, México

<sup>2</sup>Department of Physics, University of Ljubljana, Jadranska 19, 1000 Ljubljana, Slovenia

## 2. Observations

Observations were obtained with the LFOSC spectrograph at the 2.12m telescope of the Observatorio Astrofísico Guillermo Haro in Cananea, Mexico. The useful wavelength range was  $\lambda\lambda 4370 - 9000 \text{ \AA}$  and the spectral resolution was  $\sim 15 \text{ \AA}$ . The slit of 2 arcsec width was kept in the N–S direction.

The light entered the spectroscope through a frequency and phase controlled chopper. The device, described by Čadež & Galičič (1996), was used before on the same telescope to study the optical light curve of the pulsar. A blade allows light to enter the spectrograph for 10% of each pulse period. This collection window is synchronized with the pulsar and kept on the desired pulse phase interval. We use the most recent of the Jodrell-Bank monthly Crab ephemerides, translated from the Solar-System Barycentre, including real-time corrections for the Earth orbital motion. Long photometric observations confirmed that the difference between the pulsar and the chopper phase remains within  $5 \times 10^{-4}$  for at least 3 hours (Čadež et al. 2000). However the initial chopper–pulsar phase is set by maximizing the apparent magnitude of the pulsar, so that the absolute phase is only accurate to 0.03 (Galičič 1999).

Observations were obtained on Dec 13 and Dec 14 1998 and on Oct 18 and Oct 20 1999 under nearly photometric conditions and  $\sim 1''$  seeing. A total accumulated exposure on the main-pulse and the inter-pulse was 11700 sec and 9000 sec, while the total off-pulse observing time was 10200 sec. The off-pulse interval was chosen  $\simeq 0.25$  in phase after the main-pulse. Several direct images of the pulsar field were obtained in order to control the atmosphere transparency and phase of the pulsar. The wavelength calibration is generally good to  $2 \text{ \AA}$  and somewhat deteriorating at the blue end. The flux calibration, obtained through several exposures of the star EG50 and Hiltner 600, is accurate to 5% in both color and absolute fluxes. All spectra were obtained between airmasses 1.01 and 1.3. The pulsar spectra were de-reddened assuming  $E_{B-V} = A_V/3.1 = 0.51$  (Percival et al. 1993) and

$$A_\lambda/E_{B-V} = -7.51 \log(\lambda/\lambda_o) + 1.15; \quad \lambda_o = 1\mu\text{m} \quad (1)$$

which follows the average Galactic extinction curve (Savage & Mathis 1979) to better than 1% for  $0.48 < \lambda/\lambda_o < 1.0$ .

Spectra were reduced with standard IRAF routines used according to our particular purpose. First, all the spectra were aligned with respect to the tracing of the pulsar and of another star 11.4 arcsec South of the pulsar. In order to achieve an optimal flux calibration, a relatively wide aperture of 7 arcsec was used that included all pulsar-related flux and allowed for any wavelength variations of the focus of the spectrograph. All individual spectra were flux-calibrated but no nebular background was subtracted at

Table 1: Parametrization of fluxes in the 0.1-phase window centered on the main- and inter-pulse. The last line is unpulsed flux of the underlying nebular continuum in the  $1 \text{ arcsec}^2$  box centered on the pulsar.  $F_\lambda = K \times (\lambda/\lambda_o)^{-\alpha-2}$ ,  $\lambda_o = 6000 \text{ \AA}$ ,  $5000\text{\AA} < \lambda < 7500\text{\AA}$ . Fluxes are in  $\text{erg s}^{-1}/\text{cm}^2/\text{\AA}$ . All data were de-reddened using eq. 1.

	$K$	$\alpha$
main-pulse	$5.9 \times 10^{-15}$	$+0.2 \pm 0.1$
inter-pulse	$1.9 \times 10^{-15}$	$+0.2 \pm 0.1$
underlying nebula	$3.4 \times 10^{-15}$	$-0.4 \pm 0.1$

this stage. The un-pulsed light was subtracted subsequently by subtracting the off-pulse flux-calibrated spectrum obtained just before or after. This technique makes an assumption-free subtraction of any nebular light, scattered light or telluric contributions. The chopper effectively enables us to take the pulsar off the sky and subtract the nebula emission at the exact pulsar’s position. This is important as the nebular emission is varying on arcsec scale (cf. Section 4).

### 3. Pulsar

The flux-calibrated de-reddened spectra of the main-pulse and inter-pulse are presented in the upper panel of Fig. 1. The surface flux of the underlying nebula is plotted in the lower panel. Both axes are plotted in logarithmic scale.

The colors of the main-pulse and inter-pulse continuum are identical, but the nebular continuum is redder (see Table 1).

The pulsar’s spectrum features no lines apart from telluric bands and weak nebular line residuals. Note that the [OI] 5579 line is of telluric origin. The upper limits to equivalent widths of nebular lines are 5 and 10 Å for the main- and inter-pulse respectively. This translates to the very stringent limits on absolute fluxes of pulsed emission lines that are given in Table 2.

We did not find any trace of the 5920 Å absorption feature hinted by Nasuti et al. (1996). We conclude that they were right in attributing this feature to imperfect flux calibration of their spectrum.

Note that the nebular continuum is rather strong. The use of the 0.1-phase window with the chopper however suppressed it by a factor of 10. This emphasizes the advantage of our observing method.

### 4. Nebula

Davidson (1979) published the first study of selected condensations in the Crab nebula. Nasuti et al. (1996) discuss the nebular spectrum 2 arcsec East of the pulsar position. Our slit had a N–S orientation so a brief discussion of the spectrum along this direction as well as directly on the pulsar position is in order.

The shape of the (de-reddened) nebular continuum is constant along the slit ( $\alpha = -0.4 \pm 0.1$ ) except

Table 2: Upper limits to de-reddened fluxes (in  $\text{erg s}^{-1} \text{cm}^{-2}$ ) of nebular emission lines for the 0.1-phase window centered on the main- and the inter-pulse. The last column gives fluxes of nebular lines in a 2 arcsec (E-W)  $\times$  6.9 arcsec (N-S) box centered on the pulsar.

	main-pulse	inter-pulse	nebula
[ O III ] 4959+5007	$< 1.0 \times 10^{-13}$	$< 8.2 \times 10^{-14}$	$8.4 \times 10^{-12}$
[ O I ] 6300	$< 1.3 \times 10^{-14}$	$< 1.2 \times 10^{-14}$	$8.6 \times 10^{-13}$
[ O I ] 6363	$< 9.5 \times 10^{-15}$	$< 8.8 \times 10^{-15}$	$2.6 \times 10^{-13}$
H I + [ N II ] 6548-84	$< 2.5 \times 10^{-14}$	$< 3.0 \times 10^{-14}$	$4.5 \times 10^{-12}$
[ S II ] 6716+6731	$< 2.2 \times 10^{-14}$	$< 2.7 \times 10^{-14}$	$2.4 \times 10^{-12}$

for its strength. Spatial variations of surface flux continuum (de-reddened nebular continuum per square arc-sec) are shown in the lower panel of Fig. 2. The horizontal axis is the relative displacement in N-S direction with respect to the position of the pulsar and the vertical axis displays the continuum surface flux at 6000Å. There is a chance superposition of a star 11.4 arcsec South of the pulsar, so no flux is given around its position.

The upper panels of Fig. 2 give de-reddened surface fluxes of emission lines as a function of position relative to the pulsar. The lines are generally well-separated into approaching and receding components (Fig. 3). The exception is a blend of the red component of [O III] 4959 and the blue component of its 5007 counterpart which are plotted together. The H I 6563, [N II] 6548+6584 region was resolved assuming a standard 3 to 1 ratio of the [N II] line intensities.

All lines show well separated red and blue components, similar to those reported by Nasuti et al. (1996). Component velocities, given in Table 3, remain constant (to within 200 km/s) up to  $\sim 30$  arcsec from the pulsar. All lines show similar velocity shifts,  $\sim 1800$ km/s, except for the very strong receding component of [O III] 4959 and 5007 lines, receding at double velocity.

The intensity of blue and red components is highly spatially variable and uncorrelated (Fig. 2). A simple interpretation is that of an expanding shell, proposed already by Davidson (1979). The receding components of forbidden nebular lines show a wide pronounced peak  $\sim 3$  arcsec North of the pulsar. The slope of the condensation, however, extends well behind the pulsar itself. The approaching components are generally weaker and show a condensation  $\sim 4$  arcsec South of the pulsar. The kinematics and strength of  $H\alpha$  is similar to that of forbidden lines, but a pronounced receding component to the North of the pulsar is missing.

## 5. Discussion and conclusions

The main result of this work is the flux calibrated time resolved spectrum of the Crab pulsar. It shows no intrinsic spectral lines with the continuum following a power law with  $\alpha = +0.2 \pm 0.1$ . The spectra of the main-pulse and the inter-pulse are identical: flux of the main-pulse multiplied by 0.32 equals that of the inter-pulse (Fig. 4), where the formal upper limit to the difference in the power law index for the main- and the inter-pulse is 0.01 ( $2\sigma$ ).

The above value of  $\alpha$  refers to de-reddened main- and inter-pulse spectra with nebular spectra subtracted at the exact area of pulsar’s PSF. This crucial subtraction was made possible by the dedicated

Table 3: Radial velocities (in km/s) of nebular lines within 8 arc sec of the pulsar.

	Approaching			Receding		
[ O III ] 4959, 5007	-1200	$\pm$	100	+1150	$\pm$	100
[ O I ] 6300, 6363	-1050	$\pm$	200	+600	$\pm$	200
H I 6563	-1200	$\pm$	100	+650	$\pm$	100
[ N II ] 6548, 6584	-1200	$\pm$	100	+650	$\pm$	150
[ S II ] 6716, 6731	-1300	$\pm$	200	+650	$\pm$	200

chopper device that effectively enabled us to take the pulsar off the sky.

The underlying nebula is redder ( $\alpha = -0.4 \pm 0.1$ ) and of varying intensity. We expect that this fact may explain why the power law index for the pulsar spectrum reported in the literature is slightly redder than deduced here. Nasuti et al. (1996) find  $\alpha = -0.1 \pm 0.01$  in optical. Gull et al. (1998) give  $\alpha = -0.1 \pm 0.2$  (if  $E_{B-V} = 0.51$  is assumed) in the UV. Without the possibility of directly subtracting the off-pulse spectrum, one must make a model for the surrounding nebula. We simulated such modeling and took in an example the nebular spectrum 4 arcsec North and South from the pulsar as the background. This led to the derived value of  $\alpha = +0.1$  in very good seeing (FWHM  $\sim 0.7$  arcsec) or even 0.0 in more mediocre conditions. We also note that errors below 0.1 in  $\alpha$  appear unrealistic, as they imply a color calibration accurate to better than 7% – a goal difficult to achieve on a patchy nebular background and given the uncertainties in the extinction law.

We detected no color variation in the pulsed light. Photometric investigation of Eikenberry et al. (1996) reports slight color variation on pulse slopes. Note, however, that our observations were obtained close to the centers of the main- and inter-pulse. So the two studies are somewhat difficult to compare: we present flux-calibrated spectra with slightly uncertain absolute phase, while Eikenberry et al. have an excellent phase definition but lack absolute color calibration. Romani et al. (1999) report on a relative decrease of the main pulse flux in the IR ( $1.4\mu\text{m} < \lambda < 1.8\mu\text{m}$ ) with respect to the optical ( $0.38\mu\text{m} < \lambda < 0.83\mu\text{m}$ ). We can not confirm a similar trend in our optical spectra, even if the braking of the power law beyond 800 nm could possibly be interpreted in this way. Since the nebular spectrum has a similar break, we would like another independent confirmation. A phase resolved spectrum of the Crab was presented by Perryman et al. (1999). In agreement with our results they detected no color dependence of the pulse shape in the optical. Note however that a limited resolution ( $\sim 100\text{nm}$ ) and performance of the otherwise promising STJ junction detectors – together with modest seeing – prevented them from flux calibrating their spectrum and subtracting the nebular contributions.

By perfecting the stroboscopic technique we were able to obtain the spectrum of the pulsed emission of the Crab pulsar on a medium size telescope. We are now using the same technique to identify optical counterparts of known radio pulsars.

A.Č. and T.Z. acknowledge support from the Slovenian Ministry for Science and Technology. We would like to thank an anonymous referee whose comments improved the presentation of this paper.

## REFERENCES

- Čadež, A., Galičič, M. 1996, *A&A*, 306, 443
- Čadež, A., et al. 2000, in preparation
- Cocke, W. J., Disney, M. J., Taylor, D. J. 1969, *Nat*, 221, 525
- Davidson, K. 1979, *ApJ*, 228, 179
- Eikenberry, S. S., Fazio, G. G., Ransom, S. M., Middleditch, J. M., Kristian, J., Pennypacker, C. R. 1996, *ApJ*, 467, L85
- Galičič, M. 1999, PhD Thesis, University of Ljubljana

- Golden, A., Shearer, A., Beskin, G.M. 2000, ApJ Lett, in press (astro-ph/9912355)
- Gull, T. R., et al. 1998, ApJ, 495, L51
- Lundqvist, P., et al. 1999, BAAS, 194, 5207
- Lynds, R., Maran, S. P., Trumbo, D. E., 1969, ApJ, 155, L121
- Nasuti, F. P., Mignani, R., Caraveo, P. A., Bignami, G. F. 1996, A&A, 314, 849
- Percival, J. W., et al. 1993, ApJ, 407, 276
- Perryman, M. A. C., Favata, F., Peacock, A., Rando, N., Taylor, B. G. 1999, A&A, 346, L30
- Romani, R. W., Miller, A. J., Cabrera, B., Figueroa-Feliciano, E. 1999, ApJ 521, L153
- Savage, B. D., Mathis, J. S. 1979, ARA&A 17, 73

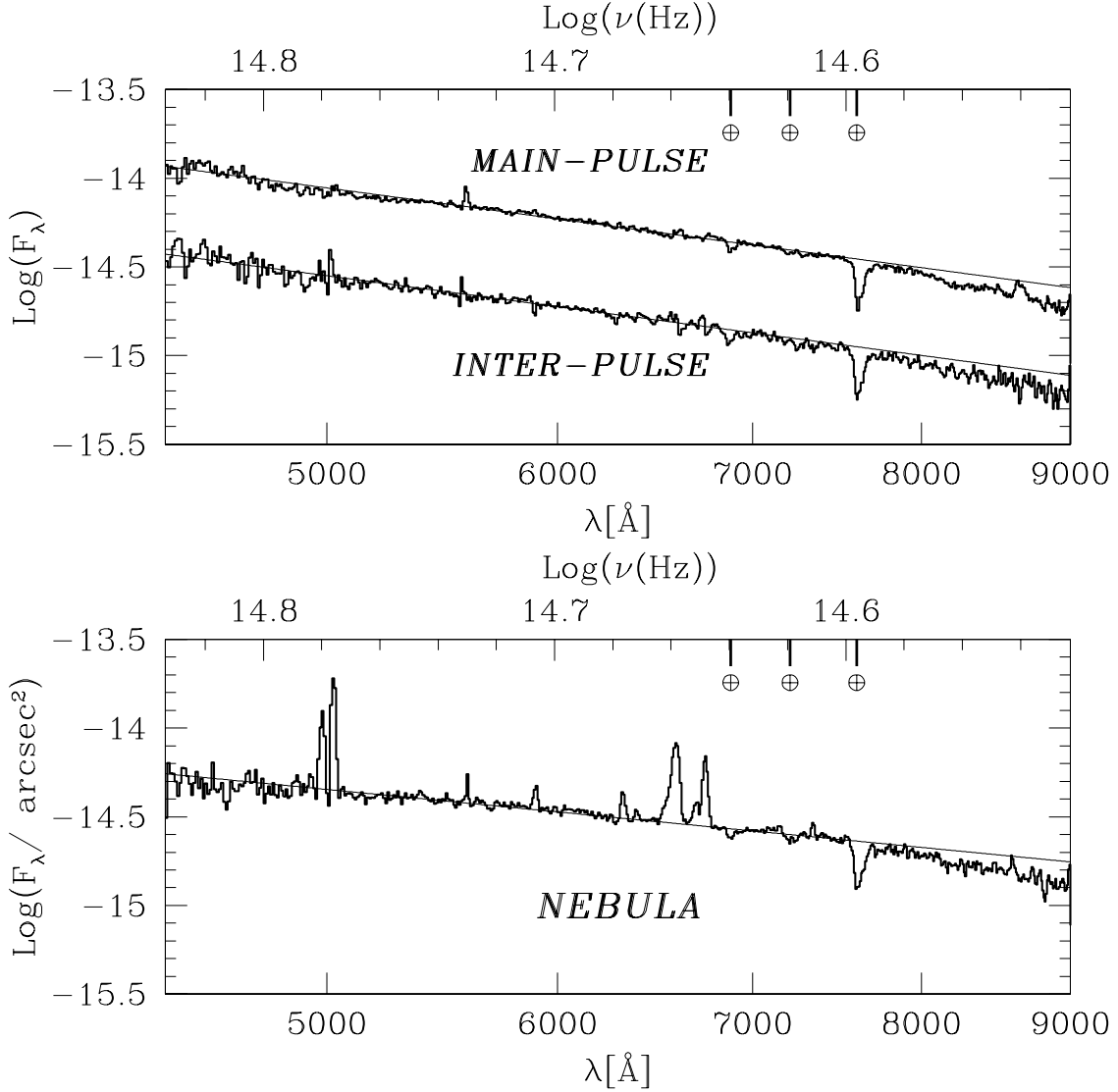


Fig. 1.— *Upper panel:*  $\text{Log}(F_\lambda) - \text{Log}(\lambda)$  spectra of the main-pulse and the inter-pulse. Emission within a 0.1 phase-window, centered on pulse’s peak, is shown. Flux is in  $\text{erg s}^{-1} \text{cm}^{-2} \text{\AA}^{-1}$ . Straight lines are power law fits (cf. Table 1).

*Lower panel:* The flux in the nebula within  $1 \text{arcsec}^2$  box centered on the pulsar.

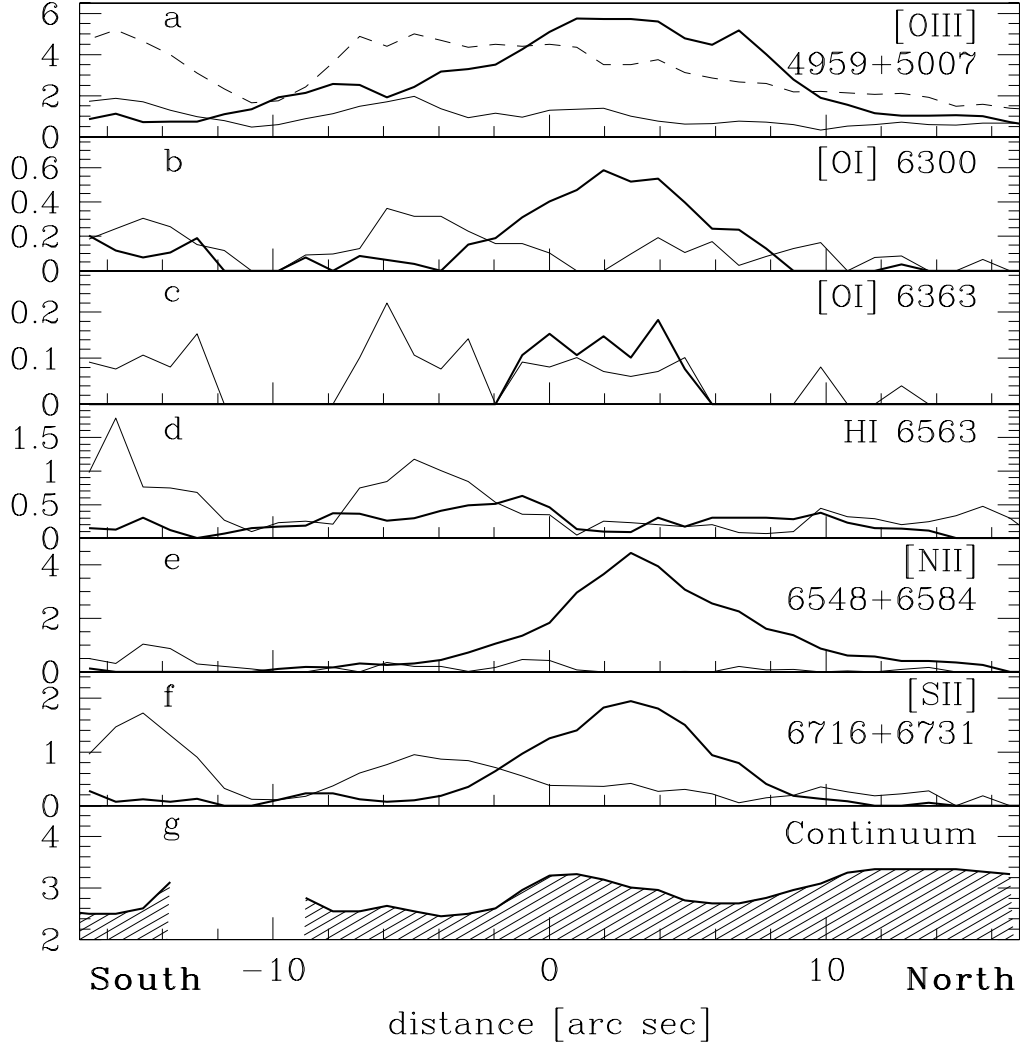


Fig. 2.— *Panels (a-f)*: Spatial variation of fluxes of the nebular emission lines. Flux is in  $10^{-13} \text{ erg s}^{-1} \text{ cm}^{-2} \text{ arcsec}^{-2}$ . The slit had a N-S orientation, distance along the slit is given with respect to the position of the pulsar. *Bold lines* refer to a receding and *normal lines* to an approaching component of each line. Components of [OIII] lines are overlapping; so we plot the receding component of 5007 [bold], the approaching of 4959 [normal] and the sum of 5007 (blueshifted) and 4959 (redshifted) [dashed line]. Flux errors are  $\sim 0.15 \times 10^{-13} \text{ erg s}^{-1} \text{ cm}^{-2} \text{ arcsec}^{-2}$  ( $2\sigma$ ), rendering them small except for the [OI] lines. *Panel (g)*: Flux in the continuum at  $6000\text{\AA}$  in units of  $10^{-15} \text{ erg s}^{-1} \text{ cm}^{-2} \text{ \AA}^{-1} \text{ arcsec}^{-2}$ . Region  $\sim 11$  arcsec south of the pulsar is omitted due to contribution of a chance superposition star.



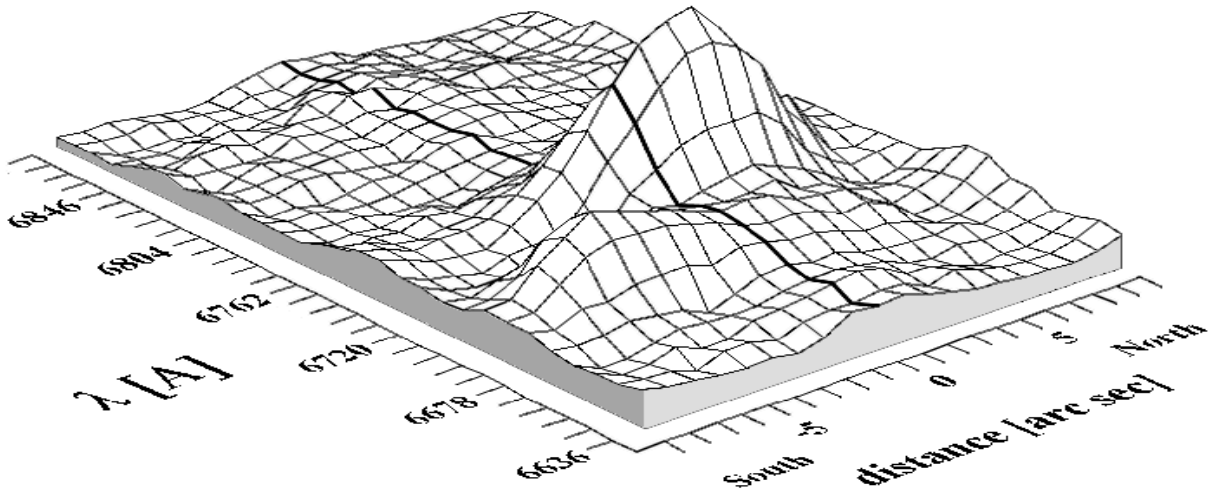


Fig. 3.— Portion of the flux calibrated spectrum of the nebula obtained with the pulsar turned off (phase  $\simeq 0.25$  after the main-pulse peak). The strong blue- and red-shifted components of the S[II] 6716+6731 doublet are seen. Their intensity varies on arc-sec scale, but their radial velocity remains constant. Thick line marks the position of the pulsar.

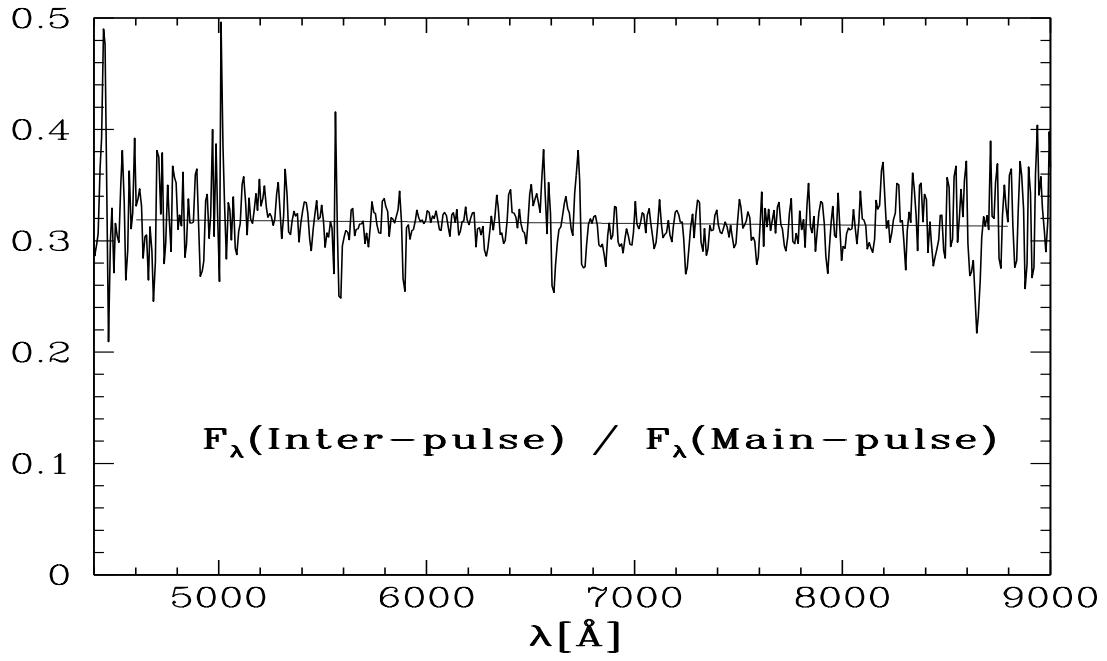


Fig. 4.— Ratio of the inter-pulse and main-pulse spectra. It is well represented with a linear fit  $0.317(1 \pm 0.003) - 0.006(1 \pm 1)(\lambda/\lambda_o - 1)$ ;  $\lambda_o = 6000 \text{ \AA}$ . Thus the spectral shapes of the main and inter-pulse in the  $4400 \text{ \AA} < \lambda < 8800 \text{ \AA}$  wavelength interval are identical.